Quantifying changes in individual-specific center-of-mass dynamics during walking with ankle exoskeletons using Hybrid-SINDy

Michael C. Rosenberg[1*], Joshua L. Proctor[1,2], Katherine M. Steele[1]

[1]Department of Mechanical Engineering, University of Washington, Seattle, United States of America
[2]Department of Applied Mathematics, University of Washington, Seattle, United States of America

* Corresponding author
Email: mcrose3@emory.edu (MCR)

Abstract

Ankle exoskeletons alter whole-body walking mechanics, energetics, and stability. Controlling the dynamics governing center-of-mass (COM) motion is critical for maintaining efficient and stable gait; these dynamics are altered following neurological injury. However, how COM dynamics change with ankle exoskeletons is unknown, and how to optimally model individual-specific COM dynamics is unclear. Here, we evaluated individual-specific changes in COM dynamics in unimpaired adults and a case study of one individual with post-stroke hemiparesis while walking in shoes-only and with zero-stiffness and high-stiffness passive ankle exoskeletons. To identify optimal sets of physically interpretable mechanisms describing COM dynamics, termed *template signatures*, we leveraged hybrid sparse identification of nonlinear dynamics (Hybrid-SINDy): an equation-free data-driven method for inferring sparse hybrid dynamics from a library of candidate functional forms. In unimpaired adults, Hybrid-SINDy automatically identified spring-loaded inverted pendulum-like template signatures, which did not change with zero- or high-stiffness exoskeletons ($p>0.13$). Conversely, post-stroke paretic leg and rotary stiffness mechanisms increased by 11% with zero- and high-stiffness exoskeletons, respectively. While unimpaired COM dynamics appear robust to passive ankle exoskeletons, how neurological injuries affect changes in COM dynamics with exoskeletons merits further investigation. Our findings also support Hybrid-SINDy's potential to discover mechanisms describing individual-specific COM dynamics with assistive devices.

Introduction

Ankle exoskeletons are prescribed and designed to improve walking function and gait mechanics[1-3]. Personalized passive and powered ankle exoskeletons have shown promise to improve walking function and muscle coordination in unimpaired adults and individuals with neurological injuries[2,4,5]. However, changes in gait in response to ankle exoskeletons are highly individualized, especially following neurological injury, making device personalization critical to improving mobility. For example, in stroke survivors and children with cerebral palsy, ankle exoskeletons elicit diverse—and sometimes detrimental—impacts on gait mechanics, walking speed, step length, and the energetic cost of walking[1-4]. Capturing and characterizing these responses remains challenging and hinders clinicians' and designers' abilities to customize exoskeletons to support walking function.

Despite observed changes in gait mechanics and energetics with ankle exoskeletons, little is known about how task-level mechanisms, such as the control of whole-body dynamics, impact exoskeleton responses[2,5-7]. Specifically, controlling center-of-mass (COM) motion is known to impact gait energetics and stability, and is related to clinical metrics of walking function and speed[8-10]. Modulating COM dynamics in response to exoskeletons may, therefore, be critical to maintaining stable and efficient gait. Importantly, following neurological injuries (*e.g.*, a stroke), COM energetics are altered asymmetrically, with the paretic limb doing less work on the COM[11]. Similarly, when walking with ankle exoskeletons, stroke survivors struggle to modulate their gait in energetically efficient ways[2]. However, these experimental studies did not quantify changes in the underlying COM dynamics with exoskeletons. Even in unimpaired adults, it is unclear whether individuals modulate COM dynamics similarly in response to exoskeletons. Characterizing the strategies used to modulate COM dynamics with ankle exoskeletons may improve our ability to explain and predict exoskeleton impacts on walking function.

Reduced-order representations of gait dynamics provide a foundation to quantify and understand complex exoskeleton responses[12-17]. For example, Full & Kodistchek (1999) used reduced-order representations of COM dynamics, such as the spring-loaded inverted pendulum (SLIP), to quantify strategies to achieve task-level goals including COM stabilization and perturbation responses during locomotion[15]. Such reduced-order representations (*i.e.*, models) of gait encode neural and biomechanical dynamics using a minimalist set of physics-based mechanisms. Specifically, common reduced-order models of COM dynamics employ a variety of mechanisms, such as the SLIP leg springs or the rigid legs of an inverted pendulum walker, and describe COM accelerations during gait[9,13,15,16,18-22]. Each mechanism within a model, therefore, encodes a hypothesis about how neural and biomechanical subsystems interact to achieve task-level objectives.

Reduced-order models of locomotion, often termed *Template* models, have provided influential insights into strategies to control COM motion to achieve stable and efficient walking. For example, inverted pendulum templates have been used to study COM energetics and the transition from walking to running[16,18], as well as strategies for energetically-efficient COM acceleration[8,22,23] and lateral stabilization[9,24]. Alternative template structures, such as the bipedal spring-loaded inverted pendulum (SLIP) and its variants further improved predictions of sagittal-plane ground reaction forces (GRFs) and revealed COM stabilization strategies across different speeds[13,20,21,25,26]. Extensions of the bipedal inverted pendulum and SLIP templates include leg damping elements, rotary springs, or curved feet. Note that each mechanism describes a unique relationship between leg kinematics and COM acceleration[19,27]. Further, given the breadth of templates proposed for human gait, the mechanisms that best describe gait are likely individual-specific. Consequently, selecting an optimal template structure to describe an individual's gait is non-trivial, particularly following neurological injury[28].

Template models that describe COM dynamics during unimpaired gait may be useful to serve as normative archetypes, from which deviations can be used to characterize altered COM dynamics.

To emphasize the individualized nature of templates, we denote the combination of mechanisms best describing individual-specific COM dynamics as a *template signature*. For example, differences in the template signatures in children with hemiparetic cerebral palsy differed from typically developing children and between legs, with increased stiffness in the paretic limb[28,29]. These differences suggested that children with cerebral palsy may have reduced dynamic resources available to control COM motion during walking, providing insight into individualized strategies to accelerate the COM and their implications for walking function.

Similarly, we may expect that template signatures will reveal altered COM dynamics following other forms of neurological injury (*e.g.*, stroke) and with ankle exoskeletons. However, characterizing changes in template signatures in these contexts requires addressing a major methodological challenge: Manually identifying optimal template signatures mechanisms is a slow, *ad hoc* process that relies on first-principles knowledge of the system[19]. The candidate template signature increases combinatorially with the number of candidate mechanisms. Therefore, new methods are needed to select mechanisms rapidly and systematically from a literature-based library of candidate mechanisms.

Recent advances in data-driven modeling and machine learning provide powerful techniques to flexibly identify system dynamics from data[30-33]. **Hybrid-SINDy** (*SINDy: Sparse identification of nonlinear dynamics*[30]) identifies sparse nonlinear dynamics in hybrid systems from time-series data, making it particularly relevant to identifying template signatures of walking, which often have distinct dynamics based on foot contact configuration[28,32]. Importantly, Hybrid-SINDy identifies a large number of candidate dynamical models (*e.g.*, template signatures) from an arbitrary library of possible functional forms (*i.e.*, mechanisms). The algorithm uses information criteria to determine levels of support for each candidate model and selects only those that are parsimonious and highly representative of the system[34]. Consequently, this approach enables rapid, systematic identification of individual-specific template signatures while leveraging first-principles knowledge of the physics of human gait.

The purpose of this study was to identify changes in template signatures in response to ankle exoskeletons and evaluate how neurological injuries may alter template signatures in response to exoskeletons. We used the Hybrid-SINDy algorithm to identify physically-interpretable, low-dimensional template signatures describing COM dynamics during walking in unimpaired adults and how those signatures changed with hinged and stiff ankle exoskeletons. We hypothesized that ankle exoskeletons would primarily increase leg stiffness. Additionally, to examine the potential of template signatures to encode changes in COM dynamics for individuals with neurological injuries, we present a case study evaluating altered template signatures in an individual with post-stroke hemiparesis.

Methods

Data collection

We collected 3D marker trajectories using a ten-camera motion capture system (Qualisys AB, Gothenburg, SE) and ground reaction forces (GRFs) using an instrumented treadmill (Bertec Inc., Columbus, USA) in twelve unimpaired adults (6M/6F; age = 23.9 ± 1.8 years; height = 1.69 ± 0.10 m; mass = 66.5 ± 11.7 kg) and one stroke survivor with lower-limb hemiparesis (*sex not disclosed*; age = 24 years; height = 1.70 m; mass = 68.0 kg). Participants walked on a treadmill in shoes-only and with bilateral passive ankle exoskeletons under two conditions: zero resistance to ankle flexion (i.e., zero stiffness; K_0) and high dorsiflexion resistance (i.e., high stiffness; K_H = 5.1 Nm/deg; Figure 1). A detailed description of the experimental protocol and data preprocessing can be found in[35]. Briefly, in a second session following a practice session, data were collected while participants walked at their self-selected speed for four minutes per condition. To mitigate fatigue, the post-stroke participant walked under the same protocol, but for only three minutes per condition[36]. This study was approved by the University of Washington Institutional Review Board (#47744). The study was performed in accordance with the approved protocol and University of Washington Institutional Review Board guidelines and regulations. All participants provided written informed consent prior to participating in the study.

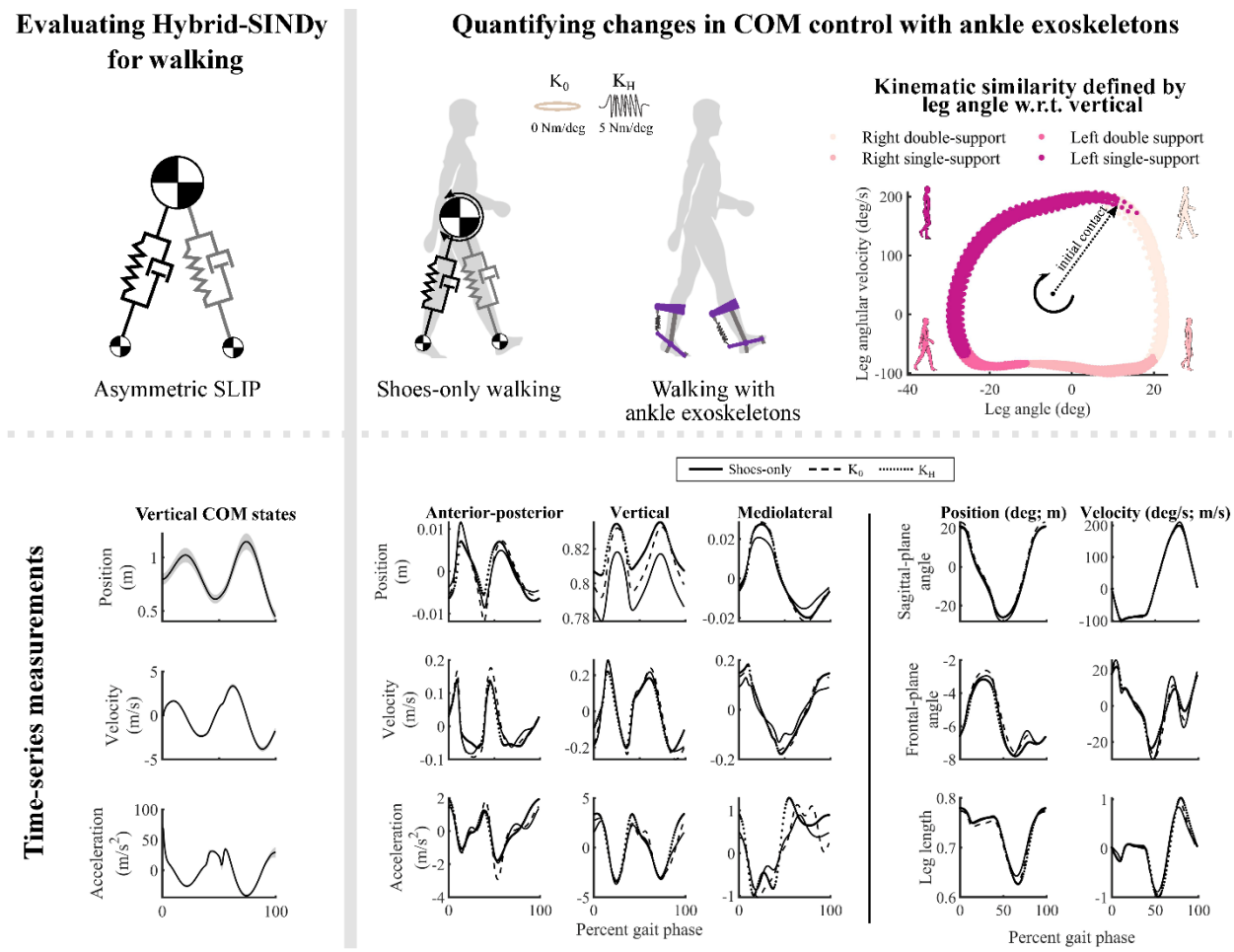

Figure 1: Model depictions and experimental data. Top: Two-dimensional depictions of the simulated SLIP (left) and human walking (right). The simulated SLIP used leg springs and dampers, as well as foot masses to simulate full strides. Participants walked on a treadmill in shoes-only and in zero- (K_0) and high-stiffness (K_H) ankle exoskeletons. The phase portrait (pink) defined a kinematic phase variable for

clustering similar measurements. Colors denote gait phases corresponding to first and second double-limb support, single-limb support, and swing. Bottom: Time-series measurements of COM position, velocity, and acceleration for the simulated SLIP (left; average ± 1SD) and an exemplary unimpaired adult participant (right). For human gait, COM states (middle) and leg states (right) are shown for each walking condition. The leg length and velocity, and sagittal- and frontal-plane leg angles determined the magnitude of forcing that the leg exerted on the COM, while COM position determined forcing direction.

Estimating template signatures with Hybrid-SINDy

We used the Hybrid-SINDy algorithm to identify template signatures during walking with and without ankle exoskeletons, separately for each walking condition. For each exoskeleton condition, we used OpenSim's *Body Kinematics* algorithm to estimate the COM and foot positions[37,38]. In this section, we describe the SINDy and Hybrid-SINDy algorithms in the context of identifying template signatures, while more detailed explanations can be found in[30] and[32]. The 3D COM accelerations, $\ddot{\boldsymbol{q}}(t) \in \mathbb{R}^{m\times n}$, were described by continuous-time nonlinear dynamics, $f\big(q(t), \dot{q}(t)\big)$, where m denotes the number of samples and n=3 denotes the output variables:

$$\frac{d^2}{dt^2}\boldsymbol{q}(t) = \ddot{\boldsymbol{q}}(t) = f\big(\boldsymbol{q}(t), \dot{\boldsymbol{q}}(t)\big), \qquad 1$$

where time is denoted by $t \in \mathbb{R}^{m\times 1}$, and $q(t)$ and $\dot{q}(t)$ represent COM positions and velocities relative to the feet, respectively, in $\mathbb{R}^{m\times n}$, in the anterior-posterior, vertical, and mediolateral directions. We assume that only a small number of functional forms (*i.e.*, mechanisms) in $f(q(t), \dot{q}(t))$ describe most of the system's behavior. We omit the time notation in the remaining sections.

Sparse Identification of Nonlinear Dynamics (SINDy)

The SINDy algorithm[30] recovers sparse nonlinear dynamics from a library of candidate functional forms, which may consist of arbitrary nonlinear functions of system measurements. Adopting the notation from[32], we can rewrite the dynamics in equation (1) as:

$$\ddot{\boldsymbol{q}} = \boldsymbol{\Theta}(\boldsymbol{q}, \dot{\boldsymbol{q}})\boldsymbol{\Xi}, \qquad 2$$

where $\Xi \in \mathbb{R}^{p\times n}$, is a linear map from nonlinear function library encoding mechanisms potentially describing COM dynamics, $\boldsymbol{\Theta}(\boldsymbol{q}, \dot{\boldsymbol{q}}) \in \mathbb{R}^{m\times p}$, to COM accelerations, $\ddot{\boldsymbol{q}}$. The coefficients in $\boldsymbol{\Xi}$, therefore, represent template signatures parameters, while $\boldsymbol{\Theta}$ encodes template signature structure. We included $p = 14$ functional forms in the function library (7 per leg), described below. The SINDy algorithm promotes sparsity using sequential least-squares regression with hard thresholding, with the threshold defined by the sparsity parameter, λ (equation 3)[32]. This thresholding approach penalizes the zero-norm of $\boldsymbol{\Xi}$ and solves:

$$\min_{\boldsymbol{\Xi}} ||\, \boldsymbol{\Theta}(\boldsymbol{q}, \dot{\boldsymbol{q}})\boldsymbol{\Xi} - \ddot{\boldsymbol{q}}||_2 + \lambda\|\boldsymbol{\Xi}\|_0, \qquad 3$$

Hybrid-SINDy

Hybrid-SINDy extends SINDy in two important ways. First, Hybrid-SINDy uses clustering to generalize SINDy to hybrid systems. For human walking, clustering enables unique dynamics to be identified in each hybrid regime, such as those defined by contact configuration (*i.e.*, single- and double-limb support)[10,14,18]. Second, Hybrid-SINDy uses information criteria to automatically select the system dynamics that best describe the data. This approach enables competing hypotheses about the mechanisms describing COM acceleration to be rapidly and systematically compared, thereby highlighting mechanisms that are common across individuals and those unique to a subset of individuals.

Applying Hybrid-SINDy to walking

We applied the Hybrid-SINDy algorithm to human gait using the following steps for each participant and walking condition (Figure 2). Note that within each hybrid regime of the gait cycle, we expanded upon the original Hybrid-SINDy algorithm by using multi-model inference to define a single template signature when multiple signatures were plausible (Step 5)[32].

1. *Clustering*: For the first 3600 samples in the training set, we generated clusters of the samples' 800 nearest neighbors and identified the centroid of each cluster. The average cluster width (7.4% of a stride) was smaller than the duration of double-limb support. We used the right leg angle and angular velocity with respect to vertical as our clustering parameters[35].

2. *Model estimation*: For each cluster, we used SINDy to identify multiple template signatures by sweeping 40 sparsity threshold values, typically producing 5-15 unique signatures per cluster.

3. *Model evaluation and selection*: Using held-out data, we evaluated the ability of each template signature to reconstruct COM accelerations in the anterior-posterior, vertical, and mediolateral directions. We computed the average reconstruction error of held-out data over gait phases, ϕ, spanning 0-100% of a stride (equation 4).

$$\text{error}_{\phi} = |\boldsymbol{\Theta}(\boldsymbol{q}, \dot{\boldsymbol{q}})\boldsymbol{\Xi} - \ddot{\mathbf{q}}|_{\phi} \qquad 4$$

We selected template signatures based on two criteria: First, we discarded signatures that were identified in less than 1% of training clusters. Frequently occurring template signatures are more likely to be robust to measurement noise or stride-to-stride variability, making them better representations of an individual's gait dynamics[32].

Second, for each hybrid regime – single- and double-limb support – we selected the frequently occurring template signatures that had the highest likelihood of being the correct signature describing COM dynamics according to the Akaike Information Criterion (AIC)[34,39]. The AIC is widely used to compare candidate representations of system dynamics (e.g., template signatures) according to their number of free parameters and log-likelihood[34]. Adopting the formulation in[32], assuming that model errors are independently, identically, and normally distributed, the AIC can be written in terms of the number of free parameters, k, number of samples, ρ, and the sum of squared residuals:

$$AIC = 2\tilde{k} + \rho \ln\left(\frac{\sum_{p=1}^{P}\sum_{i=1}^{I}\left(\hat{f}(\mathrm{q}) - \dot{q}\right)_i)^2}{\rho}\right), \qquad 5$$

where in the outer summation, P denotes the number of samples and in the inner summation, I denotes the number of output states.

The AIC favors parsimonious, highly-representative models, which is ideal for identifying minimalist representations of gait dynamics. Like Mangan and colleagues[32], we used the AIC corrected for finite sample sizes (AICc):

$$AICc = AIC + \frac{2(k+1)(k+2)}{P-k-2}. \qquad 6$$

The correction term approaches zero as the number of samples, P, increases. We then determined the relative plausibility of competing template signatures using their relative AICc score, $\Delta AICc_j$[32,34]:

$$\Delta AICc_j = AICc_{min} - AICc_j, \qquad 7$$

where $\Delta AICc_j$ represents the relative AICc score for the jth. $AICc_{min}$ represents the AICc of the model with the lowest AICc among the models compared within a hybrid regime. The best model according to the relative AICc has a score of $\Delta AICc_j = 0$ and all other models had higher scores. Burnham and Anderson noted that models with $\Delta AICc_j \leq 2$ have substantial support, while $\Delta AICc_j > 7$ have low support[34]. We adopted the threshold of[32], deeming template signatures with $\Delta AICc_j \leq 3$ to be *plausible*.

4. *Multi-model inference*: Since human gait dynamics are not strictly hybrid, multiple template signatures are likely to be deemed plausible in each hybrid regime. To construct a single template signature for each hybrid gait regime, we computed a weighted-average signature using Akaike weights, ω_j, where j is the jth plausible model in a hybrid regime[34]. Akaike weights are:

$$\omega_j = \frac{\exp\left(-\frac{\Delta \mathrm{AICc}_j}{2}\right)}{\sum_{r=1}^{R} \exp\left(-\frac{\Delta \mathrm{AICc}_r}{2}\right)}, \qquad 8$$

where $\exp\left(-\frac{\Delta AICc_j}{2}\right)$ defines the likelihood of the jth template signature given the observations[34]. This approach weights each signature based on its likelihood relative to the other plausible signatures.

5. *Uncertainty estimation*: To evaluate the robustness of the template signatures to noise and stride-to-stride variations in the data, we performed 200 bootstrapped estimates of template signatures parameters using the data in the corresponding hybrid regimes. The template signatures were characterized by the mean and standard deviation of the bootstrapped parameters.

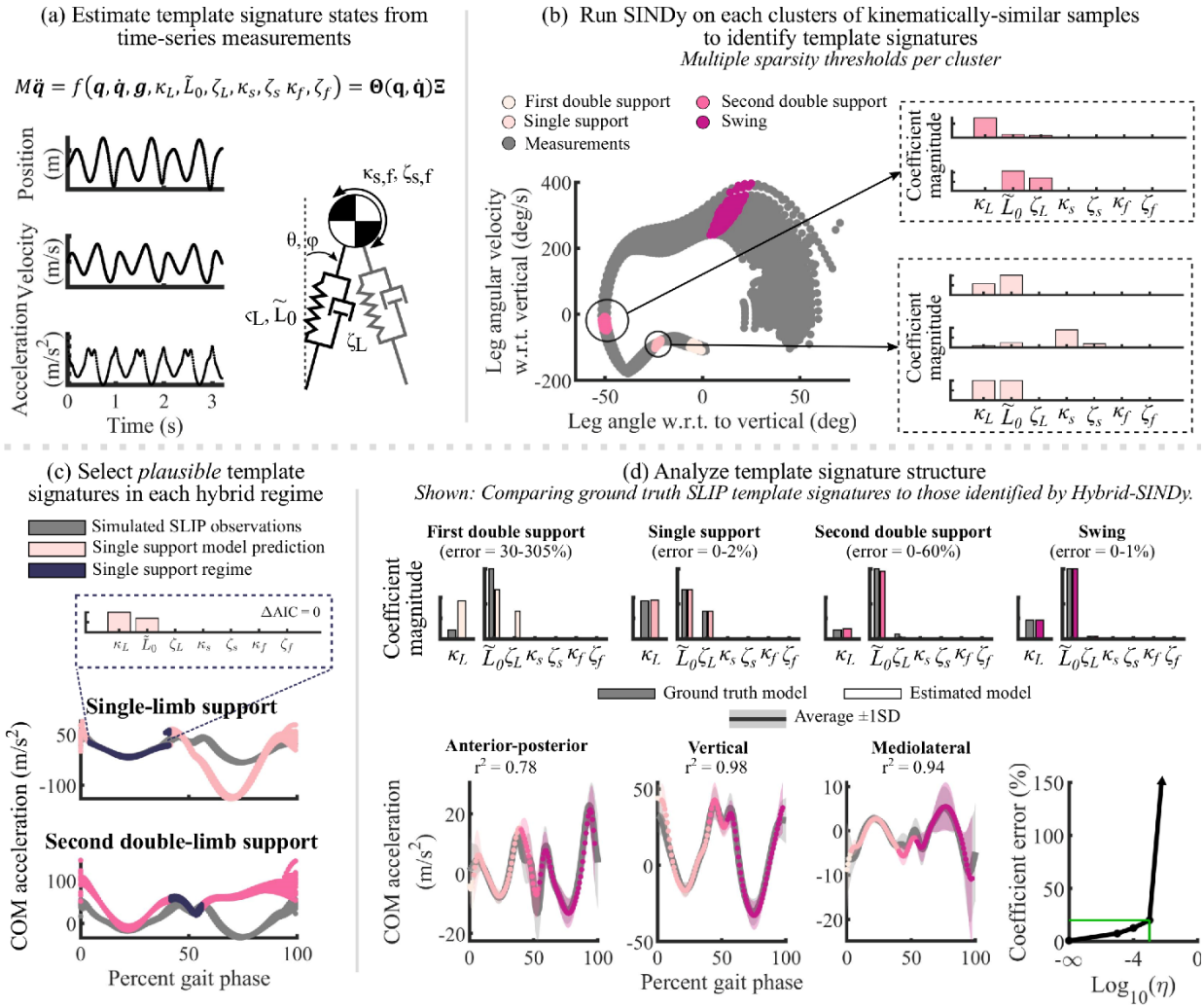

Figure 2: The Hybrid-SINDy algorithm, applied to a simulated 3D-SLIP walking model. (a) COM and foot measurements from the simulated SLIP were used to approximate nonlinear SLIP states, $\boldsymbol{\Theta}(\boldsymbol{q}, \dot{\boldsymbol{q}})$, as shown in the equation and the SLIP diagram. Variables can be found in Table 1. (b) Kinematically-similar measurements were used to cluster the data (gray) and exemplary template signature parameters from two clusters. For each cluster, multiple signatures of different complexities were identified. (c) Each signature was evaluated in the hybrid regime containing the cluster centroid. The plots show COM accelerations and predictions in single-limb (top) and second double-limb (bottom) support. Error is low only in the correct hybrid regime for each signature (purple). (d) Top: Ground-truth (gray) and identified (colors) template signatures in each hybrid regime, with percent errors compared to ground-truth. Bottom: Average (±1SD) observed (gray) and predicted (colors) COM accelerations. Colors denote each hybrid regime. The rightmost plot shows the average percent error in template signature coefficients during single-limb support and swing with increasing measurement noise (η). Green lines denote the approximate noise level of marker-based motion capture.

Template signatures mechanisms and dynamics

To model three-dimensional COM dynamics during walking, we created a function library of the following candidate mechanisms based on prior literature (Table 1):

- *Rigid legs*, which reflected pendular gait in stance[9,12,14,18,23]. Pendular gait is energetically passive and reflects kinetic and potential energy transfer during walking but cannot explain GRFs and lacks double-limb support phases[14,21,40].
- *Leg springs*[13,19-21,25] and *dampers*[27], which produce force along the leg. Leg springs are common energetically-conservative mechanisms used to describe walking and running dynamics, and enable a double-limb support phase. Leg dampers are less common, but have been used to capture non-conservative gait dynamics[27].
- *Rotary springs*[13,19] and *dampers* in the sagittal and frontal planes, which enable forcing transverse to the leg axis. The addition of rotary springs has been shown to improve reconstructions of anterior-posterior GRFs in a bipedal SLIP[19]. We did not identify rotary damping elements in prior literature but include them as a candidate mechanism describing non-conservative transverse forcing.

The mechanisms selected by the Hybrid-SINDy algorithm define the template signature *structure*, which describes characteristic strategies to accelerate the COM. The identified signature *parameters* describe each mechanism's contribution to COM accelerations.

The dynamics of a three-dimensional bipedal SLIP augmented with damping and rotary mechanisms may be written as

$$M(\ddot{\boldsymbol{q}} - \boldsymbol{g}) = \sum_{j=R,L} \left(-\left[k_L(L - L_0) + c\dot{L}\right]\frac{\boldsymbol{q}}{L} - \left[k_s\theta + c_s\dot{\theta}\right]\frac{\boldsymbol{q}}{L_s^2} - \left[k_f\phi + c_f\dot{\phi}\right]\frac{\boldsymbol{q}}{L_f^2}\right)_j, \qquad 9$$

where M is body mass, $\boldsymbol{g}$ is the gravity vector, ϕ describes the traverse-plane leg angle, and θ describes the leg angle from vertical in the direction defined by ϕ[19,25]. The summation represents the total force generated by the legs on the COM. The left-most brackets contain mechanisms that impart forces radially along the leg: k_L is the leg stiffness, L is the instantaneous leg length, L_0 is the leg resting length, c_L is the leg damping, $\dot{L}$ is the instantaneous leg velocity. We henceforth denote L_0 as *leg length* for clarity. The middle bracket contains mechanisms that impart forces transverse to the leg axis in the sagittal plane: k_s and c_s are the sagittal-plane rotary stiffness and damping, respectively. L_s denotes the sagittal-plane leg projection. Analogously in the right-most brackets, k_f and c_f represent the frontal-plane rotary stiffness and damping, respectively, and L_f denotes the frontal-plane leg projection. The derivation of system dynamics can be found in *Supplemental – S1*.

Normalized template mechanisms

To account for inter-individual differences in walking speed and body size during analysis, we normalized the template signatures (Table 1). Leg stiffness was normalized as in[17,19,32]. Leg resting length normalized to the measured leg length[19,27]. Rotary stiffness was normalized according to[19]. All damping terms were converted to damping ratios[27]. The normalized leg, sagittal-plane, and frontal-plane stiffness mechanisms are denoted by κ_L, κ_s, and κ_f, respectively. The normalized leg, sagittal-plane, and frontal-plane damping mechanisms are denoted by ζ_L, ζ_s, and ζ, respectively. Normalized leg length is denoted $\tilde{L}_0$. We can rewrite equation (9) as a linear combination of our normalized coefficients and nonlinear transformations of our states:

$$M(\ddot{\boldsymbol{q}} - \boldsymbol{g}) = [\kappa_L \quad \kappa_L\tilde{L}_0 \quad \zeta_L \quad \kappa_s \quad \zeta_s \quad \kappa_f \quad \zeta_f]_j\, \boldsymbol{\Theta}(\boldsymbol{q}, \dot{\boldsymbol{q}}), \quad j = \{Right, Left\} \qquad 10$$

The COM position and velocity relative to the feet were used to compute candidate template signature states: leg lengths and lengthening velocities, sagittal-plane leg angles and angular velocities relative to vertical, and frontal-plane leg angles and angular velocities relative to vertical. The complete function library can be found in *Supplemental – S1*.

Table 1 – Template signature functional forms.

Term	Symbol	Normalized form
Leg stiffness	κ_L	$\frac{k_L L_{bio}}{Mg}$
Leg resting length	$\tilde{L}_0$	L_0/L_{bio}
Leg damping	ζ_L	$\frac{c_L}{2\sqrt{k_L M}}$
Sagittal-plane rotary stiffness	κ_s	$\frac{k_s}{MgL_{bio}}$
Sagittal-plane rotary damping	ζ_s	$\frac{c_s}{\sqrt{\kappa_s M L_{bio}^2}}$
Frontal-plane rotary stiffness	κ_f	$\frac{k_f}{MgL_{bio}}$
Frontal-plane rotary damping	ζ_f	$\frac{c_f}{\sqrt{\kappa_f M L_{bio}^2}}$

c_L=leg damping; c_s=sagittal-plane rotary damping; c_f=frontal-plane rotary damping; g = gravitational acceleration; k_L=leg stiffness; k_s=sagittal-plane rotary stiffness; k_f=sagittal-plane rotary stiffness; L_{bio} = biological leg length; M = body mass

Evaluating Hybrid-SINDy's ability to select template signatures

To evaluate Hybrid-SINDy's ability to accurately identify and select walking dynamics, we evaluated the algorithm on synthetic data of a simulated bipedal SLIP walker with known dynamics (Figure 1 & Figure **2**)[25]. The bipedal SLIP had asymmetric leg stiffness and damping, and masses representing the pelvis (M = 56 kg) and feet (M_f = 7 kg) to simulate a full gait cycle (Table 2). We omitted rotary mechanisms from the SLIP dynamics but used the full function library described in equation (9). To replicate the human walking datasets, we simulated 120 gait cycles from randomly perturbed initial conditions with an average initial velocity of 1.20 m/s. As SINDy's performance is sensitive to sensor noise, we identified template signatures using simulation measurements with Gaussian noise ranging logarithmically from 10 nm to 10 cm added to the position measurements[30]. We quantified the Hybrid-SINDy's ability to reconstruct model dynamics using the number of correctly-selected mechanisms and the accuracy of estimated coefficients.

Table 2 – Bipedal SLIP normalized simulation parameters.

Term	*[Right leg, Left leg]*			
	DS_1	**SS**	**DS_2**	**SW**
κ_L	[10.8, 9.1]	[25.1, 18.82]	[9.03, 10.68]	[36.6,25.3]
$\tilde{L}_0$	[1.0, 1.0]	[1.0, 0.7]	[1.0, 1.0]	[0.7, 0.7]
ζ_L	[0.04, -0.07]	[-0.03, -0.04]	[0, 0]	[-0.40, -0.57]
κ_s	0	0	0	0
ζ_s	0	0	0	0
κ_f	0	0	0	0
ζ_f	0	0	0	0

Identifying template signatures in human gait

We estimated unique template signatures that predicted COM accelerations using the Hybrid-SINDy algorithm for each participant and ankle exoskeleton condition. 10800 samples (90 seconds) were available for clustering, and we identified template signatures for the first 3600 samples. An additional 3600 samples of held-out data were used for model evaluation and selection.

To evaluate the extent to which each mechanism described COM accelerations in unimpaired adults, we determined the proportion of participants for whom each template signature coefficient was selected. Signature terms that are identified across individuals represent mechanisms fundamental to COM dynamics, while infrequently identified mechanisms describe individual-specific features of COM dynamics.

To determine if unimpaired COM dynamics during shoes-only walking generalized to walking with ankle exoskeletons, we evaluated the ability of shoe-walking template signature structures to reconstruct COM accelerations in the K_0 and K_H conditions. We used least-squares regression to identify template signature parameters for the K_0 and K_H conditions using the shoes-only template signature structure. We compared the relative AICc scores ($\Delta AICc$) between these signature structures and those of the signature structures specific to the K_0 and K_H trials. To determine if shoes-only template signatures were less plausible (*i.e.*, $\Delta AICc \geq 3$) than signature structures selected for the K_0 and K_H conditions, we compared shoes-only relative AICc scores to those of the K_0 and K_H conditions using one-sample paired t-tests ($\alpha = 0.05$).

To determine if the ankle exoskeleton frame or mass impacted COM dynamics, we compared template signature coefficients between the K_0 and Shoe conditions. Similarly, to evaluate the impacts of exoskeleton stiffness on COM dynamics, we compared template signature coefficients in the K_H and K_0 conditions. For both comparisons, we used paired two-sample t-tests with Holm-Sidak step-down corrections for multiple comparisons ($\alpha = 0.05$)[41]. Because shoes-only template signature structures were plausible for most unimpaired participants, we used the shoes-only template signatures structure to estimate signature coefficients across walking conditions.

To determine if COM dynamics may be altered post-stroke, we computed the percent difference in the non-paretic and paretic limb template signature parameters during shoes-only walking in one individual with post-stroke hemiparesis. We also evaluated changes in post-stroke COM dynamics with ankle exoskeletons by computing percent changes in template signature coefficients for the K_0 condition compared to the shoes-only and K_H conditions.

Results

The Hybrid-SINDy algorithm correctly identified the salient features of the simulated SLIP's template signature during single-limb support (Figure 2). Specifically, Hybrid-SINDy identified non-zero leg stiffness (κ_L), resting length ($\tilde{L}$), and damping (ζ_L) terms only – consistent with the SLIP's dynamics. In the noise-free condition, 86% of terms were correctly selected and only one term, leg damping in first double-limb support, was incorrectly selected. Both double-limb support regimes were very short in the simulated SLIP: 1.3% and 4.6% of samples in first and second double-limb support – smaller than the 7.4% of the training data in each cluster. Consequently, all clusters with centroids in the double-limb support regimes contained samples spanning double- and single-limb support. Hybrid-SINDy incorrectly omitted only damping terms with small coefficients (Table 2). Without measurement noise, in single-limb support and swing, coefficients were within 2% of the ground truth values. When measurement noise with a standard deviation of 1 mm – similar to that of our motion capture system – was added to the system measurements, Hybrid-SINDy correctly selected only 63% of mechanisms, though incorrect mechanisms selection occurred primarily in double-limb support. Template signature coefficients were estimated with an average error of less than 29% in single-limb support and swing (Figure 2). In single-limb support, Hybrid-SINDy was still able to estimate large coefficients (*i.e.*, leg stiffness and resting length) with less than 1% error.

When walking in shoes-only, template signatures reveal individual-specific and common strategies to accelerate the COM across unimpaired participants. In both double-limb and single-limb support, SLIP mechanisms – leg stiffness and leg length – were selected in 96-100% of limbs (Figure 3). Unimpaired template signatures were not significantly different between legs (paired 2-sample t-test; $p > 0.01$). However, template signatures varied during double-limb support: Rotary stiffness terms were selected in 58-67% of limbs in the first double-limb support and 83-95% of limbs during second double-limb support. Except for sagittal-plane damping, damping terms were selected in less than 20% of limbs. As expected during swing, when the limb should not contribute to COM accelerations, no terms were selected. We, therefore, omitted the swing regime from remaining analyses.

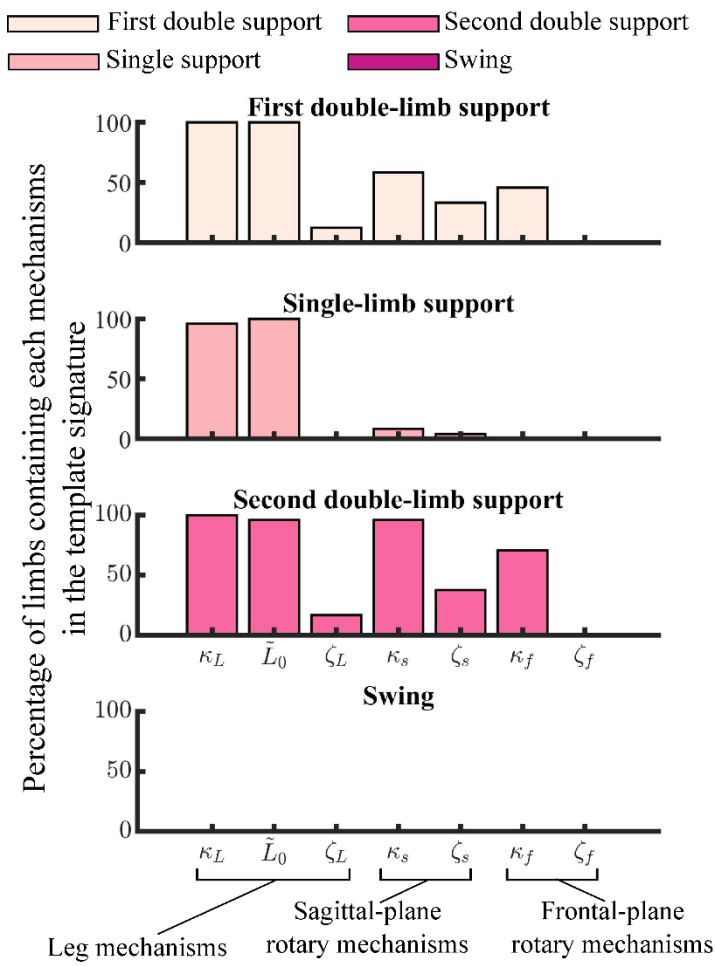

Figure 3: The percentage of unimpaired limbs whose template signatures contained each mechanism in each hybrid regime. For 24 limbs, the percent of limbs for which each template signature mechanism was selected by the Hybrid-SINDy algorithm. Colors denote each hybrid regime. Mechanisms selected in a larger percentage of legs suggest common representations of COM dynamics, while less frequently selected mechanisms reflect individual-specific features describing COM dynamics.

For each unimpaired participant, template signatures were robust to stride-to-stride variations during single-limb support: bootstrapped stiffness and leg length coefficients had coefficients of variation (CVs) less than 0.021 ± 0.015. In both double-limb support phases, CVs of stiffness and sagittal-plane rotary damping coefficients ranged from 0.11–0.26. Less-frequently selected mechanisms in double-limb support – leg damping and frontal-plane damping – were more variable than frequently selected mechanisms, with CVs ranging from 0.082–0.442.

Across unimpaired participants, single-limb support leg length was the least variable coefficient (CV = 0.03), while leg stiffness differed more between participants (CV = 0.28; Figure 4; top). Interindividual variability in double-limb support leg and rotary stiffness was larger than single-limb support coefficients (CV = 0.43–1.94). Despite interindividual differences in template signature coefficients, signatures reconstructed participants' COM accelerations well, explaining 32-85% of the variance in 3D COM accelerations (Figure 4; bottom).

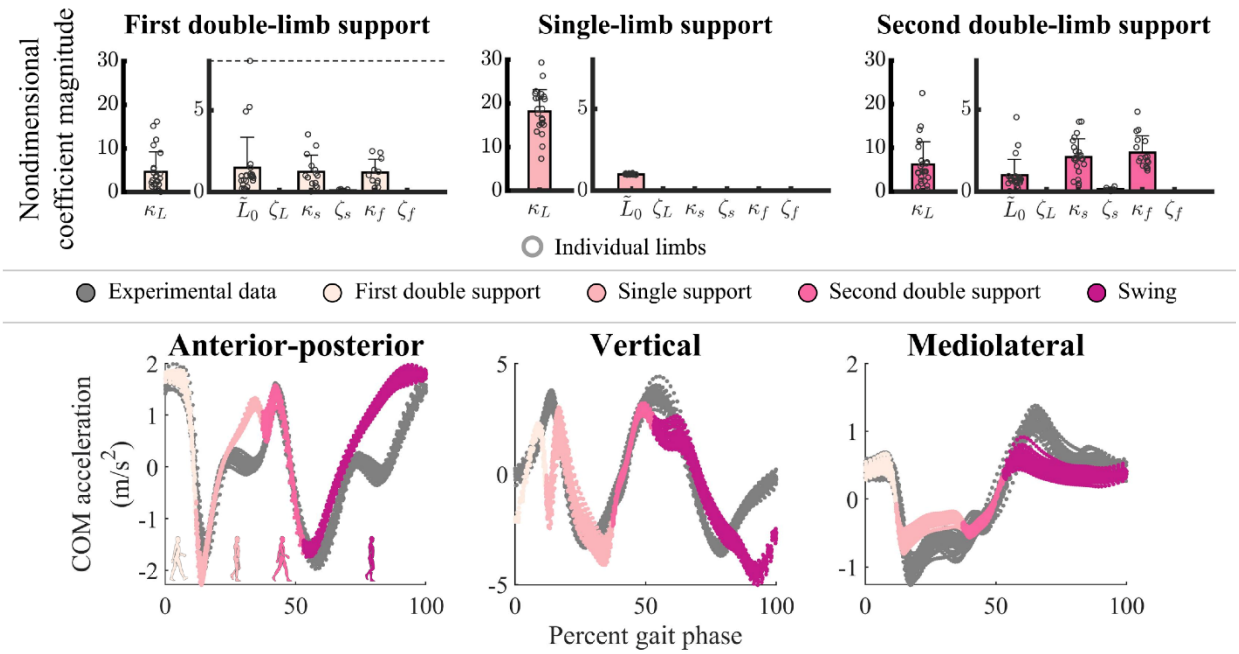

Figure 4: Unimpaired template signatures of walking in shoes-only. Normalized template signatures (top) and reconstructed COM accelerations (bottom) for shoes-only walking in each hybrid regime. Top: Bars denote the average template signature (+1SD) in single- and double-limb support. The small circles represent individual limbs. Note that we omitted mechanisms that were selected in less than 25% of participants. The dashed lines truncate large terms for clarity. Bottom: Experimental and predicted COM accelerations from the test dataset of an exemplary unimpaired participant. The gray dots denote the experimental accelerations, while the colors correspond to predictions in each hybrid regime.

Passive ankle exoskeletons elicited only small changes in unimpaired COM dynamics: in single-limb support, the shoes-only template signature structures reconstructed K_0 and K_H COM dynamics with similar accuracy to template signature structures fit specifically for the K_0 ($\Delta AICc = 0.2 \pm 0.7$; p = 0.29) and K_H ($\Delta AICc = 0.7 \pm 2.9$; p = 0.24) conditions, respectively (Figure 5; top). Conversely, in double-limb support, shoes-only signatures did not consistently reconstruct K_0 or K_H COM dynamics, with relative AICc scores ranging from $-118 \leq \Delta AICc < 220$. The negative relative AICc scores occurred when the shoes-only template signature structure was never identified by Hybrid-SINDy in the exoskeleton conditions. Therefore, to compare signature coefficients between exoskeleton conditions, we constrained each participant's template signatures to that selected in the shoes-only condition.

Using this approach, we found that no unimpaired template signature coefficients changed significantly when walking in shoes-only, zero-stiffness exoskeletons (K_0), and stiff exoskeletons (K_H) ($p > 0.05$). Specific to our hypothesis, we found that neither ankle exoskeleton mass and frame (K_0) nor stiffness (K_H) had a significant impact on leg stiffness in any gait phase ($p > 0.13$) (Figure 5; bottom).

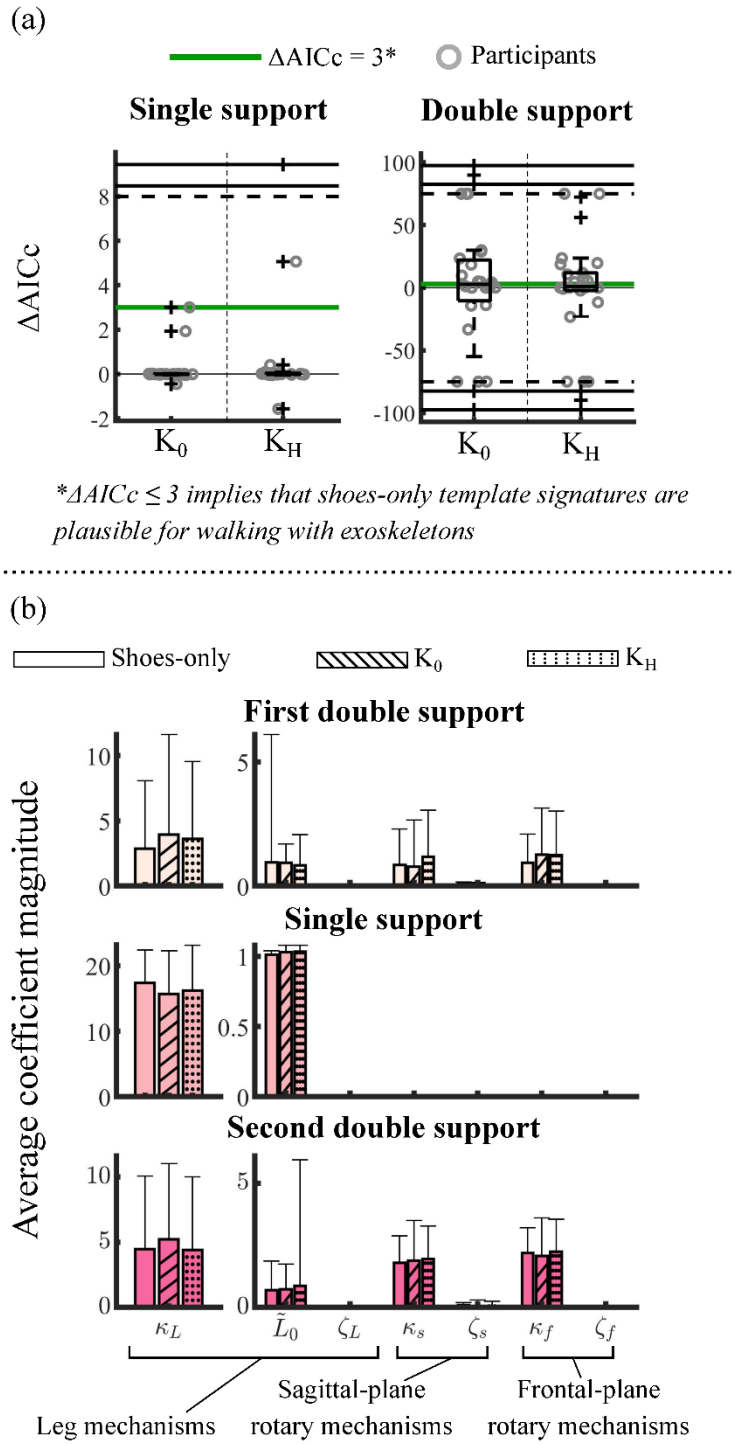

Figure 5: Changes in template signatures with ankle exoskeletons. (a) Relative AICc ($\Delta AICc$) between template signatures identified specifically for the K_0 and K_H conditions, and signatures constrained to the shoes-only signature structures. Positive $\Delta AICc$ values indicate that shoes-only signature structures were less plausible than those identified specifically for each condition. $\Delta AICc$ scores are shown for single-limb support (left) and double-limb support (right). $\Delta AICc \leq 3$ (green lines) denote plausible shoe template signature structures. For double-limb support, large $\Delta AICc$ scores

are truncated at $\Delta AICc = \pm 75$ for clarity. (b) Template signatures of walking in shoes only (solid bars), zero-stiffness (K_0; slashed bars) exoskeletons, and high-stiffness exoskeletons (K_H; dotted bars) during single- and double-limb support. Bars represent the average (+1SD) template signature across participants. Leg stiffness (κ_L) is included on a separate subplot for clarity. The large variability in leg length during double-limb support is due to one limb with a high resting length.

Unlike unimpaired adults, one stroke survivor's shoes-only template signature revealed distinct strategies for accelerating the COM in double, but not single-limb support. The template signature structure was symmetric between the paretic and non-paretic limbs during single-limb support, consisting of only leg stiffness and resting length (Figure 6). However, the paretic limb was 31% stiffer than the non-paretic limb. Conversely, template signature structure was asymmetric in double-limb support, with rotary stiffness mechanisms selected as a mechanism explaining COM dynamics in only the paretic limb. During first double-limb support, leg damping and rotary stiffness were selected in only the paretic limb. In second double-limb support, both paretic and non-paretic rotary stiffness mechanisms were selected. Due to asymmetric template signature structures, we did not compare shoes-only signature coefficients between legs in double-limb support.

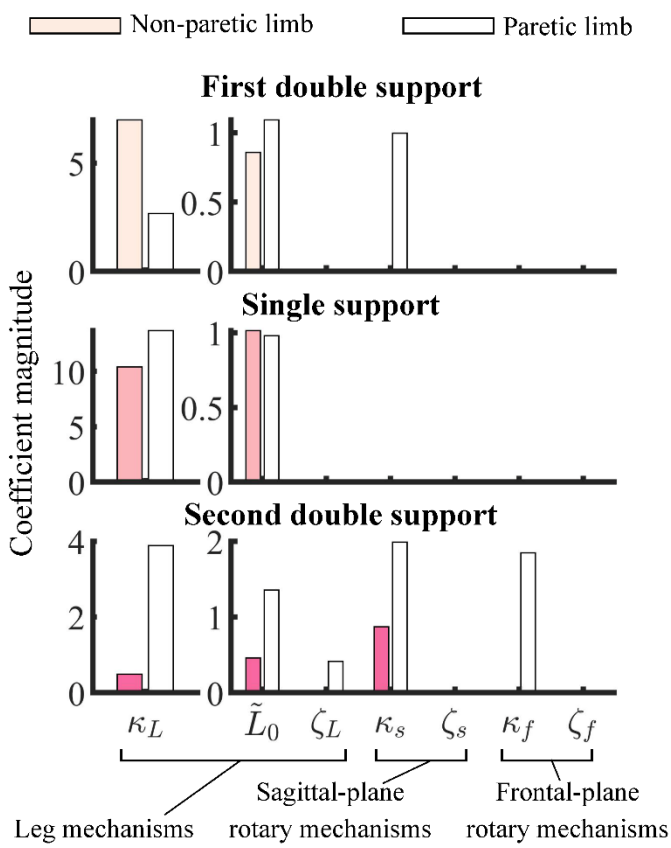

Figure 6: Inter-limb differences in template signatures in one stroke survivor. Non-paretic (colored bars) and paretic (white bars) template signatures for one individual with post-stroke hemiparesis. This participant's template signatures differed in the paretic and non-paretic limbs in double-limb support, as shown by the zero-values for non-paretic sagittal-plane rotary stiffness in first double-limb support (top row) and the leg damping and frontal-plane stiffness in double-limb support (third row).

The exoskeleton mass and frame (Shoe vs. K_0) primarily impacted the stroke survivor's paretic leg stiffness and non-paretic leg rotary stiffness. Compared to walking in shoes-only, paretic leg stiffness was 11% greater in the zero-stiffness (K_0) exoskeleton condition in single-limb support and over twice as stiff in double-limb support (Figure 7; slashed bars vs. no bars). Responses to the K_0 exoskeleton condition were asymmetric, with the non-paretic leg being slightly (3%) less stiff in the K_0 condition than the shoes-only condition in single-limb support, while sagittal-plane rotary stiffness was 41% larger in second double-limb support. Conversely, exoskeleton stiffness (K_0 vs. K_H) had small impacts on paretic-leg template signatures. In the high-stiffness (K_H) exoskeleton condition, single-limb support paretic leg stiffness was only 1% larger than in the K_0 condition (Figure 7; dotted vs, slashed bars). Both paretic and non-paretic leg rotary stiffness were 11% greater in second double limb support than in the K_0 condition. Non-paretic leg stiffness was 49% smaller than with zero-stiffness (K_0) exoskeletons in single-limb support.

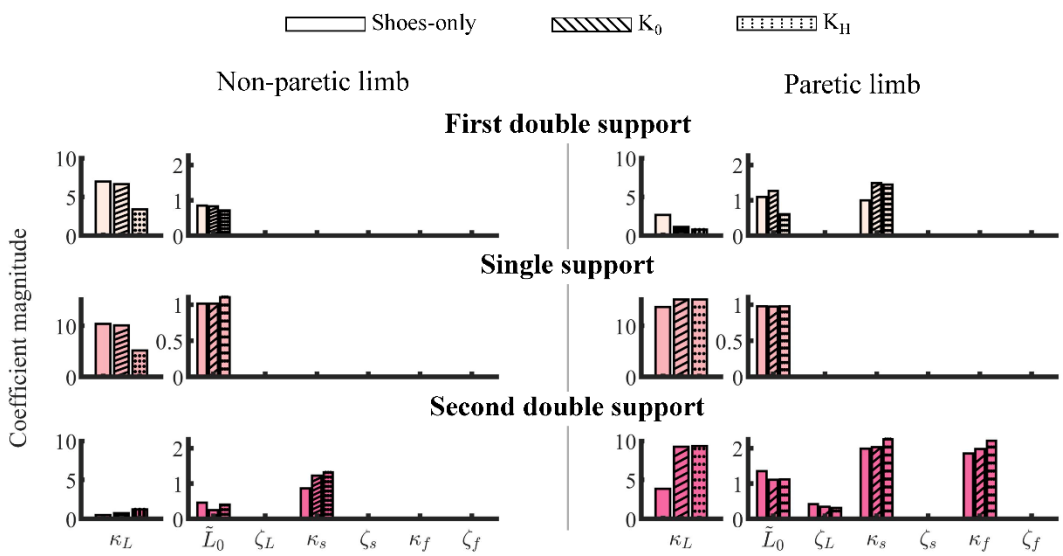

Figure 7: Template signatures of one stroke survivor walking with and without ankle exoskeletons. Bars denote template signatures in the shoes-only (clear bars), zero-stiffness (K_0; slashed bars), and high-stiffness (K_H; dotted bars) ankle exoskeleton conditions for the non-paretic (left) and paretic (right) limbs. Bars represent the average template signatures over 200 bootstrapped model fitting iterations. Colors correspond to each hybrid regime.

Discussion

We evaluated the impacts of passive ankle exoskeletons on individual-specific COM dynamics – described by template signatures – using a recently-developed data-driven modeling framework, Hybrid-SINDy. Using synthetic data generated by forward simulations of SLIP dynamics, we showed that Hybrid-SINDy could accurately identify COM dynamics at measurement noise levels comparable to marker-based motion capture. Therefore, the template signatures identified by Hybrid-SINDy for human gait likely encoded meaningful information about exoskeleton impacts on COM dynamics. When applied to human walking data, the symmetric and SLIP-like unimpaired shoes-only template signatures automatically selected by Hybrid-SINDy were consistent with prior models of walking dynamics, but suggest that dynamics described by rotary mechanisms are individual-specific[19,25]. Conversely, our post-stroke case study's asymmetric shoes-only signatures showcase Hybrid-SINDy's ability to identify pathological COM dynamics[28]. Contrary to our hypothesis, unimpaired COM dynamics were robust to the mechanical constraints of passive ankle exoskeletons: frame and mass, and dorsiflexion stiffness. Larger changes in template signatures with exoskeletons in our post-stroke case study, however, suggest that neurological or biomechanical constraints may limit the ability to maintain shoes-only COM dynamics with ankle exoskeletons. Understanding how individual-specific COM dynamics change with exoskeletons or other assistive devices may improve clinicians' and researchers' abilities to personalize such devices to enhance mobility.

Unimpaired and post-stroke template signatures highlighted inter-individual differences in COM dynamics. The uniform selection of SLIP mechanisms (leg stiffness and resting length) from data is consistent with common template walking models and supports the perspective that elastic legs are foundational mechanisms for describing COM accelerations during walking across unimpaired individuals[12,20,21,25,42]. Conversely, our finding that rotary mechanisms were selected to describe COM dynamics in only 50% of limbs may explain their less frequent application in template walking models[13,19]. Each template signature mechanism describes distinct coordination patterns between leg kinematics and COM accelerations. SLIP mechanisms may describe coordination patterns necessary for stable or efficient walking, while rotary mechanisms describe coordination patterns that have smaller, more individualized impacts on gait. Determining which mechanisms of COM dynamics predict individual differences in exoskeleton responses or walking function represents an interesting area of future research.

In our case study of one stroke survivor, asymmetric template signatures suggest that inter-limb differences in COM dynamics can be automatically identified from data. Consistent with template-based studies in children with cerebral palsy, the post-stroke participant's paretic leg was stiffer than the nonparetic leg in single- and second double-limb support[28,29]. Increased paretic leg stiffness may reflect a more pendular gait or increased co-contraction in the paretic leg[43]. Similarly, in first double-limb support, the selection of sagittal-plane rotary stiffness and damping mechanisms is consistent with experimental observations that the paretic leg does greater negative work than the non-paretic limb during loading response in stroke survivors[11]. These results highlight the potential functional interpretability of data-driven template signatures and the importance of leg-specific parameterizations of COM dynamics to understand how the legs contribute differentially to COM accelerations following neurological injury.

Contrary to our primary hypothesis that unimpaired leg stiffness would change with stiff ankle exoskeletons, unimpaired COM dynamics appear robust to altered ankle constraints due to passive ankle exoskeletons despite observed changes in kinematics and muscle activity[35]. Similarly, Collins and colleagues (2015) observed small changes in total COM power with passive ankle exoskeletons compared to walking in shoes-only, but larger changes in biological contributions to COM power[5]. Our findings suggest that these small changes in COM power could be driven by altered COM *kinematics*, rather than changes in the underlying COM *dynamics*. Maintaining COM dynamics with different ankle exoskeleton

properties requires modulating joint or muscle-level (*i.e.*, execution-level) dynamics, which may be altered following neurological injury[5,7,28,35,44].

Our post-stroke case study—in which template signatures changed with exoskeleton frame and stiffness—supports the potential impacts of neurological injuries on the ability to modulate COM dynamics with exoskeletons. Unlike unimpaired adults, paretic limb sagittal-plane rotary stiffness in first double-limb support and leg stiffness in single-limb support increased with the exoskeleton mass and frame (K_0 vs. shoes-only). Increased paretic-leg stiffness may stem from the exoskeleton frame restricting excessive inversion of the paretic ankle, which the participant noted during data collection. Conversely, minimal impacts of the exoskeleton stiffness on the paretic limb template signatures (K_H vs. K_0) during single-limb support suggests that, for this participant, exoskeleton stiffness did not alter body weight support strategies[45]. Rather, increased paretic-leg rotary stiffness during double-limb support suggests that exoskeleton stiffness primarily altered the dynamics of forcing transverse to the leg, potentially altering propulsion or stabilization dynamics by serving a similar role to the ankle plantarflexors[46-48]. We emphasize that the specific findings from this case study are unlikely to generalize across a larger cohort of stroke survivors with diverse gait deficits: individual-specific neural or biomechanical constraints may alter the ability to modulate joint-level dynamics to convert exoskeleton assistance into functionally relevant forcing[2]. Nonetheless, this case study highlights Hybrid-SINDy's potential to discover interpretable changes in post-stroke COM dynamics with exoskeletons.

The Hybrid-SINDy algorithm[32,33] was essential to discovering individual-specific and leg-specific changes in COM dynamics with ankle exoskeletons in the present study. By automatically identifying and selecting different first principles-based representations of COM dynamics, we rapidly compared competing hypotheses about human gait dynamics. Conversely, manually comparing all possible template signatures for our fourteen-dimensional mechanism library would require a combinatorially-large number of models to be generated, fit, and compared. Using a principled approach to model identification and selection, Hybrid-SINDy selected dynamics that are consistent with literature in a fraction of the time required to manually compare each candidate model. While Hybrid-SINDy has primarily been applied to synthetic systems, this work supports its ability to capture dynamics from real human gait data.

While alternative approaches could identify similar template signatures, Hybrid-SINDy provides unique insight into the structure of COM dynamics. Our approach is similar to one study in bipedal locomotion that used multi-layer optimization to select human-like template dynamics for walking robot controllers[49]. Hybrid-SINDy extends this approach by using information criteria to enable multiple highly-plausible representations of walking dynamics to be selected and analyzed for an individual[34,39]. For most participants, the Hybrid-SINDy algorithm identified a single plausible template signature in each hybrid regime, indicating that alternative hypothetical representations of COM dynamics lacked strong statistical support. If multiple plausible template signatures were identified for an individual, new experiments could be designed to better differentiate between plausible signatures.

Hybrid-SINDy's ability to identify template signatures from forward simulations of a synthetic SLIP model with known dynamics at moderate noise levels suggests that individual differences in template signatures of human gait data reflect differences in COM dynamics. Hybrid-SINDy performed as expected in the noise-free condition, accurately identifying single-limb support and swing dynamics, except for small damping terms. Terms with small contributions to system behavior, such as damping in this study, may be omitted by the AICc in favor of parsimony[34,39]. An important implication of this result is that Hybrid-SINDy will not always select the true system dynamics but will select terms critical to describing the salient behavior of the system. In our human walking data, Hybrid-SINDy may, therefore, have omitted mechanisms describing subtle idiosyncrasies in COM dynamics that could be important for gait stability or efficiency. Future experiments using different constraints or perturbations may identify additional mechanisms needed to describe COM dynamics. The reduced accuracy of synthetic SLIP

template signatures in double-limb support and with increasing noise magnitude is consistent with results of Hybrid-SINDy applied to a spring-mass hopper and supports our use of 800 samples per cluster[32]. However, long time-series datasets are needed to ensure that clusters are small enough to span only a single hybrid regime but large enough to remain robust to sensor noise.

The limitations of Hybrid-SINDy based template signatures of COM dynamics should constrain the interpretation of our findings, particularly as reduced-order representations of complex dynamical processes. Human gait dynamics are continuously phase-varying rather than hybrid, such that template signatures may vary continuously over the gait cycle. Our preliminary analyses found that plausible models' abilities to reconstruct COM dynamics diverged near the transitions between single and double-limb support, suggesting that changes in dynamics between foot contact configurations are larger than changes within configurations. Consequently, pre-defining hybrid regimes based on contact configuration was reasonable and consistent with existing hybrid template models of walking[19,20,25,32]. Additionally, we evaluated only a subset of mechanisms that could describe COM dynamics. While we chose a subset of physically-meaningful mechanisms from literature[17,19-21,25,27], future studies could derive more-nuanced insight into the structure of COM dynamics using larger mechanism libraries. Similarly, we assumed that COM dynamics were time-invariant, though COM dynamics may change with adaptation to exoskeletons[50]. We included a two-minute adaptation period for each walking condition, but additional adaptation may mask changes in participants' template signatures. Identifying the plausibility of template signatures across trials could improve our understanding of how COM dynamics change during adaptation. Finally, our limited sample size may have masked exoskeleton impacts on unimpaired gait. Rotary stiffness terms appeared to increase slightly with exoskeletons but did not reach significance. Our post-stroke case study only provides a proof-of-concept that highlights how ankle exoskeletons may elicit changes in pathological COM dynamics. Evaluating template signatures on larger unimpaired and post-stroke cohorts is needed to understand how COM dynamics change following neurological injury.

This work presents an early application of physics-informed data-driven modeling techniques to study human gait dynamics with broad applications in human movement research. Integrating principles from biomechanics and neuromechanics with *interpretable* data-driven modeling techniques like Hybrid-SINDy may accelerate the discovery of mechanisms underlying diverse movement patterns in human locomotion. Hybrid-SINDy may be leveraged to characterize changes in COM dynamics across arbitrary interventions or walking conditions, such as with powered exoskeletons. Changes in gait kinematics and kinetics with our passive ankle exoskeletons were smaller than those observed with powered exoskeletons[2,6,35]. Larger exoskeleton perturbations may elicit changes in not just the magnitude of template signature coefficients, but also signature structure, which may serve as design or control variables for powered exoskeletons aiming to enhance stability or agility[51]. In a clinical context, our case study suggests that quantifying patient-specific changes in COM dynamics may improve our ability to characterize gait deficits and explain heterogeneous immediate or longitudinal responses to assistive devices or treatment paradigms in individuals with neurological injuries[2,28,50].

Conclusions

We quantified changes in individual-specific COM dynamics in response to passive ankle exoskeletons using a physics-informed data-driven modeling framework, Hybrid-SINDy. Hybrid-SINDy successfully constructed characteristic template signatures during walking by identifying mechanisms describing the salient features of an individual's COM dynamics. Unimpaired adults maintained nearly invariant COM dynamics with ankle exoskeletons, while exoskeletons altered COM dynamics in one individual post-stroke. These findings provide insight into control of whole-body walking dynamics with ankle exoskeletons and extend a powerful data-driven modeling tool to human locomotion.

Data Availability

All experimental data and modeling code used in this study are freely available at https://simtk.org/projects/ankleexopred.

Competing interests

The authors declare no competing interests.

Funding

This material is based upon work supported by the National Science Foundation (https://nsf.gov/) under grant no. CBET-1452646 to Katherine. M. Steele, the National Science Foundation Graduate Research Fellowship Program (https://www.nsfgrfp.org/) under grant no. DGE-1762114 to Michael. C. Rosenberg, and a University of Washington Gatzert Child Welfare Fellowship (https://grad.uw.edu/graduate-student-funding/funding-information-for-students/fellowships/list-of-fellowships/gatzert-child-welfare-fellowship/) to Michael. C. Rosenberg. The funders had no role in study design, data collection and analysis, decision to publish, or preparation of the manuscript.

Author contributions

M.C.R., K.M.S. and J.L.P. contributed equally to the conception and design of this work and to the interpretation of results. M.C.R. collected data, conducted all analyses, created figures, and wrote the initial manuscript draft. J.L.P. provided theoretical guidance on the implementation of the Hybrid-SINDy algorithm. K.M.S. provided experimental resources and guidance on the analysis of gait with exoskeletons. All authors contributed to substantive revisions of the manuscript.

References

1 Kerkum, Y. L. *et al.* The effects of varying ankle foot orthosis stiffness on gait in children with spastic cerebral palsy who walk with excessive knee flexion. *PloS one* **10**, e0142878 (2015).

2 McCain, E. M. *et al.* Mechanics and energetics of post-stroke walking aided by a powered ankle exoskeleton with speed-adaptive myoelectric control. *Journal of neuroengineering and rehabilitation* **16**, 1-12 (2019).

3 Ries, A. J., Novacheck, T. F. & Schwartz, M. H. The efficacy of ankle-foot orthoses on improving the gait of children with diplegic cerebral palsy: a multiple outcome analysis. *PM&R* **7**, 922-929 (2015).

4 Lerner, Z. F., Harvey, T. A. & Lawson, J. L. A Battery-Powered Ankle Exoskeleton Improves Gait Mechanics in a Feasibility Study of Individuals with Cerebral Palsy. *Annals of biomedical engineering* **47**, 1345-1356 (2019).

5 Collins, S. H., Wiggin, M. B. & Sawicki, G. S. Reducing the energy cost of human walking using an unpowered exoskeleton. *Nature* **522**, 212-215 (2015).

6 Jackson, R. W., Dembia, C. L., Delp, S. L. & Collins, S. H. Muscle–tendon mechanics explain unexpected effects of exoskeleton assistance on metabolic rate during walking. *Journal of Experimental Biology* **220**, 2082-2095 (2017).

7 Sawicki, G. S. & Khan, N. S. A Simple Model to Estimate Plantarflexor Muscle–Tendon Mechanics and Energetics During Walking With Elastic Ankle Exoskeletons. *IEEE Transactions on Biomedical Engineering* **63**, 914-923 (2016).

8 Donelan, J. M., Kram, R. & Kuo, A. D. Mechanical work for step-to-step transitions is a major determinant of the metabolic cost of human walking. *Journal of Experimental Biology* **205**, 3717-3727 (2002).

9 Kuo, A. D. Stabilization of Lateral Motion in Passive Dynamic Walking. *The International Journal of Robotics Research* **18**, 917-930, doi:10.1177/02783649922066655 (1999).

10 Kuo, A. D. The six determinants of gait and the inverted pendulum analogy: A dynamic walking perspective. *Human movement science* **26**, 617-656 (2007).

11 Farris, D. J., Hampton, A., Lewek, M. D. & Sawicki, G. S. Revisiting the mechanics and energetics of walking in individuals with chronic hemiparesis following stroke: from individual limbs to lower limb joints. *Journal of neuroengineering and rehabilitation* **12**, 1-12 (2015).

12 Alexander, R. M. Simple models of human movement. (1995).

13 Davoodi, A., Mohseni, O., Seyfarth, A. & Sharbafi, M. A. From template to anchors: transfer of virtual pendulum posture control balance template to adaptive neuromuscular gait model increases walking stability. *Royal Society open science* **6**, 181911 (2019).

14 McGeer, T. Passive dynamic walking. *I. J. Robotic Res.* **9**, 62-82 (1990).

15 Full, R. J. & Koditschek, D. E. Templates and anchors: neuromechanical hypotheses of legged locomotion on land. *Journal of experimental biology* **202**, 3325-3332 (1999).

16 Cavagna, G. A., Heglund, N. C. & Taylor, C. R. Mechanical work in terrestrial locomotion: two basic mechanisms for minimizing energy expenditure. *American Journal of Physiology-Regulatory, Integrative and Comparative Physiology* **233**, R243-R261 (1977).

17 Holmes, P., Full, R. J., Koditschek, D. & Guckenheimer, J. The dynamics of legged locomotion: Models, analyses, and challenges. *SIAM review* **48**, 207-304 (2006).

18 Srinivasan, M. & Ruina, A. Computer optimization of a minimal biped model discovers walking and running. *Nature* **439**, 72 (2006).

19 Antoniak, G. *et al.* Spring-loaded inverted pendulum goes through two contraction-extension cycles during the single-support phase of walking. *Biology open* **8** (2019).

20 Lipfert, S. W., Günther, M., Renjewski, D., Grimmer, S. & Seyfarth, A. A model-experiment comparison of system dynamics for human walking and running. *Journal of theoretical biology* **292**, 11-17 (2012).
21 Maus, H.-M., Lipfert, S., Gross, M., Rummel, J. & Seyfarth, A. Upright human gait did not provide a major mechanical challenge for our ancestors. *Nature communications* **1**, 1-6 (2010).
22 Garcia, M., Chatterjee, A., Ruina, A. & Coleman, M. The simplest walking model: stability, complexity, and scaling. (1998).
23 Buczek, F. L. *et al.* Performance of an inverted pendulum model directly applied to normal human gait. *Clinical Biomechanics* **21**, 288-296 (2006).
24 Donelan, J. M., Shipman, D. W., Kram, R. & Kuo, A. D. Mechanical and metabolic requirements for active lateral stabilization in human walking. *Journal of biomechanics* **37**, 827-835 (2004).
25 Geyer, H., Seyfarth, A. & Blickhan, R. Compliant leg behaviour explains basic dynamics of walking and running. *Proceedings of the Royal Society B: Biological Sciences* **273**, 2861-2867 (2006).
26 Dingwell, J. B. & Cusumano, J. P. Humans use multi-objective control to regulate lateral foot placement when walking. *PLoS computational biology* **15**, e1006850 (2019).
27 Kim, S. & Park, S. Leg stiffness increases with speed to modulate gait frequency and propulsion energy. *Journal of Biomechanics* **44**, 1253-1258, doi:https://doi.org/10.1016/j.jbiomech.2011.02.072 (2011).
28 Holt, K. G., Fonseca, S. T. & LaFiandra, M. E. The dynamics of gait in children with spastic hemiplegic cerebral palsy: theoretical and clinical implications. *Human Movement Science* **19**, 375-405 (2000).
29 Fonseca, S. r. T., Holt, K. G., Fetters, L. & Saltzman, E. Dynamic resources used in ambulation by children with spastic hemiplegic cerebral palsy: relationship to kinematics, energetics, and asymmetries. *Physical Therapy* **84**, 344-354 (2004).
30 Brunton, S. L., Proctor, J. L. & Kutz, J. N. Discovering governing equations from data by sparse identification of nonlinear dynamical systems. *Proceedings of the National Academy of Sciences* **113**, 3932-3937 (2016).
31 Brunton, S. L. & Kutz, J. N. *Data-driven science and engineering: Machine learning, dynamical systems, and control*. (Cambridge University Press, 2019).
32 Mangan, N. M., Askham, T., Brunton, S. L., Kutz, J. N. & Proctor, J. L. Model selection for hybrid dynamical systems via sparse regression. *Proceedings of the Royal Society A* **475**, 20180534 (2019).
33 Mangan, N. M., Kutz, J. N., Brunton, S. L. & Proctor, J. L. Model selection for dynamical systems via sparse regression and information criteria. *Proceedings of the Royal Society A: Mathematical, Physical and Engineering Sciences* **473**, 20170009 (2017).
34 Anderson, D. & Burnham, K. Model selection and multi-model inference. *Second. NY: Springer-Verlag* **63** (2004).
35 Rosenberg, M. C., Banjanin, B. S., Burden, S. A. & Steele, K. M. Predicting walking response to ankle exoskeletons using data-driven models. *Journal of the Royal Society Interface* **17**, 20200487 (2020).
36 Genthe, K. *et al.* Effects of real-time gait biofeedback on paretic propulsion and gait biomechanics in individuals post-stroke. *Topics in stroke rehabilitation* **25**, 186-193 (2018).
37 Delp, S. L. *et al.* OpenSim: open-source software to create and analyze dynamic simulations of movement. *IEEE transactions on biomedical engineering* **54**, 1940-1950 (2007).
38 Rajagopal, A. *et al.* Full-body musculoskeletal model for muscle-driven simulation of human gait. *IEEE transactions on biomedical engineering* **63**, 2068-2079 (2016).
39 Akaike, H. in *Selected Papers of Hirotugu Akaike* 215-222 (Springer, 1974).

40 Lee, C. R. & Farley, C. T. Determinants of the center of mass trajectory in human walking and running. *Journal of experimental biology* **201**, 2935-2944 (1998).
41 Glantz, S. (New York: McGraw-Hill, 2012).
42 Mochon, S. & McMahon, T. A. Ballistic walking. *Journal of biomechanics* **13**, 49-57 (1980).
43 Clark, D. J., Ting, L. H., Zajac, F. E., Neptune, R. R. & Kautz, S. A. Merging of Healthy Motor Modules Predicts Reduced Locomotor Performance and Muscle Coordination Complexity Post-Stroke. *Journal of Neurophysiology* **103**, 844-857, doi:10.1152/jn.00825.2009 (2010).
44 Steele, K. M., Jackson, R. W., Shuman, B. R. & Collins, S. H. Muscle recruitment and coordination with an ankle exoskeleton. *Journal of biomechanics* **59**, 50-58 (2017).
45 Neptune, R. R., Clark, D. J. & Kautz, S. A. Modular control of human walking: a simulation study. *Journal of biomechanics* **42**, 1282-1287 (2009).
46 Neptune, R. R., Kautz, S. A. & Zajac, F. E. Contributions of the individual ankle plantar flexors to support, forward progression and swing initiation during walking. *Journal of biomechanics* **34**, 1387-1398 (2001).
47 Pandy, M. G., Lin, Y.-C. & Kim, H. J. Muscle coordination of mediolateral balance in normal walking. *Journal of Biomechanics* **43**, 2055-2064, doi:http://dx.doi.org/10.1016/j.jbiomech.2010.04.010 (2010).
48 Kim, M. & Collins, S. H. in *Rehabilitation Robotics (ICORR), 2013 IEEE International Conference on.* 1-6 (IEEE).
49 Chen, Y.-M. & Posa, M. in *2020 IEEE International Conference on Robotics and Automation (ICRA).* 8753-8760 (IEEE).
50 Seethapathi, N., Clark, B. & Srinivasan, M. Exploration-based learning of a step to step controller predicts locomotor adaptation. *bioRxiv*, 2021.2003.2018.435986, doi:10.1101/2021.03.18.435986 (2021).
51 Sawicki, G. S., Beck, O. N., Kang, I. & Young, A. J. The exoskeleton expansion: improving walking and running economy. *Journal of NeuroEngineering and Rehabilitation* **17**, 25, doi:10.1186/s12984-020-00663-9 (2020).